

In-medium \bar{K} - and η -meson interactions and bound states*

AVRAHAM GAL, ELI FRIEDMAN, NIR BARNEA

Racah Institute of Physics, The Hebrew University
Jerusalem 91904, Israel

AND

ALEŠ CIEPLÝ, JIŘÍ MAREŠ, DANIEL GAZDA†

Nuclear Physics Institute, 25068 Řež, Czech Republic

The role played by subthreshold meson-baryon dynamics is demonstrated in K^- -atom, \bar{K} -nuclear and η -nuclear bound-state calculations within in-medium models of $\bar{K}N$ and ηN interactions. New analyses of kaonic atom data reveal appreciable multi-nucleon contributions. Calculations of η -nuclear bound states show, in particular, that the ηN scattering length is not a useful indicator of whether or not η mesons bind in nuclei nor of the widths anticipated for such states.

PACS numbers: 13.75.Gx, 13.75.Jz, 21.65.Jk, 21.85.+d

1. Introduction

The near-threshold $\bar{K}N$ and ηN scattering amplitudes are both attractive and energy dependent in models that generate dynamically the nearby meson-baryon s -wave resonances $\Lambda(1405)$ and $N^*(1535)$, respectively. Although free-space hadron-nucleon attraction at threshold appears to be a necessary condition for binding hadrons in nuclei, careful consideration of medium modifications is required to turn it into a sufficient condition. For example, it was pointed out by Wycech and others in the early 1970s that *subthreshold* K^-N scattering amplitudes are the relevant ones even for studies of kaonic atoms, in spite of the kaon energy essentially being at threshold [1, 2, 3]. Yet, systematic treatments of energy dependence within dynamical and self-consistent calculations of \bar{K} and η bound states in nuclei

* Presented by Avraham Gal at the II International Symposium on Mesic Nuclei, Cracow, September 22-24 2013.

† Present address: ECT*, Villa Tambosi, I-38123 Villazzano (Trento), Italy.

have been lacking until recently. The present overview is focused on recent progress made by the Prague-Jerusalem Collaboration towards incorporating medium modifications, particularly those implied by the energy dependence of the corresponding scattering amplitudes [4, 5, 6, 7, 8, 9, 10, 11].

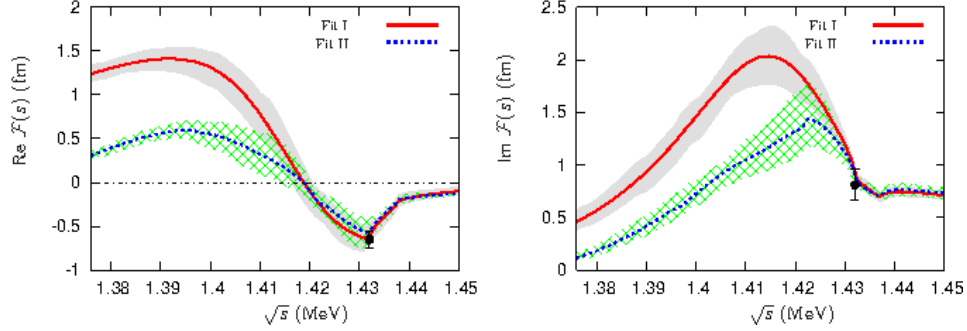


Fig. 1. Real (left panel) and imaginary (right panel) parts of the K^-p center-of-mass (cm) scattering amplitudes generated in two NLO chiral-model fits [12]. The K^-p threshold values marked by solid dots follow from the SIDDHARTA measurement of kaonic hydrogen $1s$ level shift and width [13]. Figure adapted from Ref. [12].

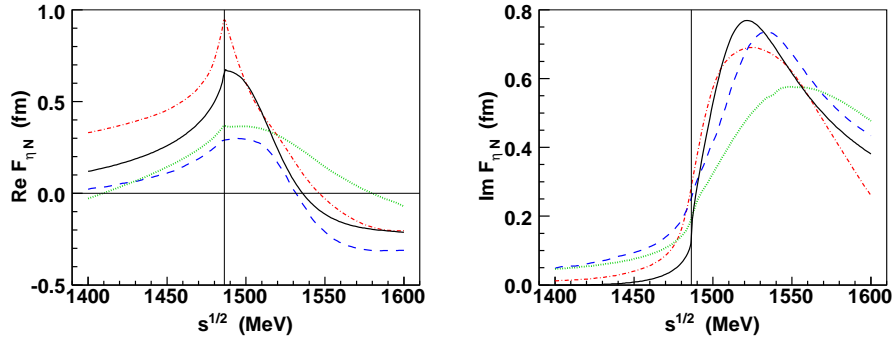


Fig. 2. Real (left panel) and imaginary (right panel) parts of the ηN cm scattering amplitude $F_{\eta N}(\sqrt{s})$ as a function of the total cm energy \sqrt{s} in four meson-baryon coupled-channel interaction models. In decreasing order of $\text{Re } a_{\eta N}$: dot-dashed, GW [14]; solid, CS [15]; dotted, M2 [16]; dashed, IOV [17]. The thin vertical line denotes the ηN threshold.

The first point worth noting about subthreshold scattering amplitudes is that they are highly model dependent. This is demonstrated for K^-p in Fig. 1 and for ηN in Fig. 2. For K^-p the two NLO chiral-model fits by Guo and Oller [12] to scattering and reaction data above and at threshold

generate scattering amplitudes, shown in Fig. 1, that differ substantially from each other in the subthreshold region. Fit-I amplitude is quite similar to those found in NLO fits by Ikeda, Hyodo and Weise (IHW) [18] and by Cieplý and Smejkal (CS) [19] both of which were used in recent K^- -atom calculations [7, 9]. For ηN the four scattering amplitudes shown in Fig. 2 differ below as well as above the ηN threshold, with perhaps just one common value $a_{\eta N} \approx 0.2 - 0.3$ fm for the imaginary part at threshold.

The present overview is organized as follows. In-medium meson-baryon scattering amplitudes are discussed in Sect. 2, for both $\bar{K}N$ and ηN , focusing on the connection between their (subthreshold) energy and density dependencies. The use of such in-medium K^-N scattering amplitudes in kaonic-atom calculations and fits is discussed in Sect. 3. Related applications to kaonic bound-state calculations are discussed in Sect. 4 for few-body systems, and in Sect. 5 for many-body systems. For η mesons, nuclear bound-state calculations using in-medium energy and density dependent ηN amplitudes are discussed in Sect. 6. A brief summary and outlook in Sect. 7 concludes this presentation.

2. In-medium amplitudes and energy versus density dependence

The in-medium modifications of free-space scattering amplitudes become particularly transparent by working with separable interactions. In Refs. [15, 19] Cieplý and Smejkal introduced meson-baryon coupled-channel energy-dependent separable s -wave interactions matched to SU(3) chiral scattering amplitudes in up to next-to-leading order (NLO) of the chiral expansion. The Tomozawa-Weinberg leading order (LO) term provides a good approximation for $\bar{K}N$ [19], but going to NLO is mandatory for ηN [15] since the relevant data involve dominantly the πN channel which is decoupled from ηN at LO. Solving the in-medium coupled-channel Lippmann-Schwinger equations $F = V + VGF$ with these potential kernels leads to a separable form of in-medium scattering amplitudes F_{ij} , given in the two-body cm system by

$$F_{ij}(k, k'; \sqrt{s}, \rho) = g_i(k^2) f_{ij}(\sqrt{s}, \rho) g_j(k'^2), \quad (1)$$

with momentum-space form factors $g_j(k^2)$, where j runs over channels, and in-medium reduced amplitudes $f_{ij}(\sqrt{s}, \rho)$ expressed as

$$f_{ij}(\sqrt{s}, \rho) = \left[(1 - v(\sqrt{s}) \cdot G(\sqrt{s}, \rho))^{-1} \cdot v(\sqrt{s}) \right]_{ij}. \quad (2)$$

Here, G is a channel-diagonal Green's function in the nuclear medium:

$$G_n(\sqrt{s}, \rho) = -4\pi \int_{\Omega_n(\rho)} \frac{d^3p}{(2\pi)^3} \frac{g_n^2(p^2)}{k_n^2 - p^2 - \Pi^{(n)}(\sqrt{s}, \rho) + i0}, \quad (3)$$

where the integration on intermediate meson-baryon momenta is limited to a region $\Omega_n(\rho)$ ensuring that the intermediate nucleon energy is above the Fermi level in channels n involving nucleons. The self-energy $\Pi^{(n)}(\sqrt{s}, \rho)$ stands for the sum of hadron self-energies in channel n . Of particular interest is the meson (h) self-energy $\Pi_h^{(hN)} = (E_N/\sqrt{s})\Pi_h$ in the diagonal $n \equiv (hN)$ channel, where the lab self-energy Π_h is given by

$$\Pi_h(\sqrt{s}, \rho) \equiv 2\omega_h V_h = -\frac{\sqrt{s}}{E_N} 4\pi F_{hN}(\sqrt{s}, \rho) \rho, \quad (4)$$

depending implicitly on $\omega_h = m_h - B_h$ and on the off-shell two-body momenta k, k' . This self-energy, once evaluated *self-consistently* while converting its \sqrt{s} dependence into a full density dependence, serves as input to the Klein-Gordon bound-state equation

$$[\nabla^2 + \tilde{\omega}_h^2 - m_h^2 - \Pi_h(\omega_h, \rho)] \psi = 0, \quad (5)$$

in which $\tilde{\omega}_h = \omega_h - i\Gamma_h/2$, with B_h and Γ_h the binding energy and the width of the meson-nuclear bound state, respectively.

In-medium amplitudes above and below threshold are shown in Fig. 3 for K^-N [19] and ηN [15]. The K^-N real part of the amplitude is strongly attractive, of order 1 fm at subthreshold energies that according to the discussion below are relevant to K^- atomic and nuclear states. The attraction as well as the absorptivity expressed by the imaginary part of the amplitude get moderately weaker for $\rho \geq 0.5\rho_0$, as demonstrated by comparing on the left panel the solid curves ($\rho = \rho_0$) with the dashed curves ($\rho = 0.5\rho_0$). In contrast, the ηN real part decreases substantially upon going below subthreshold, with values in the range of 0.1–0.2 fm, with little density dependence. This implies that K^- bound states are very likely to exist, whereas η nuclear states may not bind. Similarly, the widths generated by the imaginary part of the scattering amplitudes are considerably larger for K^- than for η mesons.

To determine the subthreshold energies for use in in-medium hadron-nucleon scattering amplitudes, we recall that the Mandelstam variable s is given by $s = (\sqrt{s_{\text{th}}} - B_h - B_N)^2 - (\vec{p}_h + \vec{p}_N)^2$, where $\sqrt{s_{\text{th}}} \equiv m_h + m_N$ and B_h and B_N are meson and nucleon binding energies. Since $\vec{p}_h + \vec{p}_N \neq 0$ in the meson-nuclear cm frame (approximately the lab frame), the associated negative contribution to s has to be included. To leading order in binding energies and kinetic energies with respect to rest masses, the downward energy shift $\delta\sqrt{s} \equiv \sqrt{s} - \sqrt{s_{\text{th}}}$ is expressed as

$$\delta\sqrt{s} \approx -B_N - B_h - \xi_N \frac{p_N^2}{2m_N} - \xi_h \frac{p_h^2}{2m_h}, \quad (6)$$

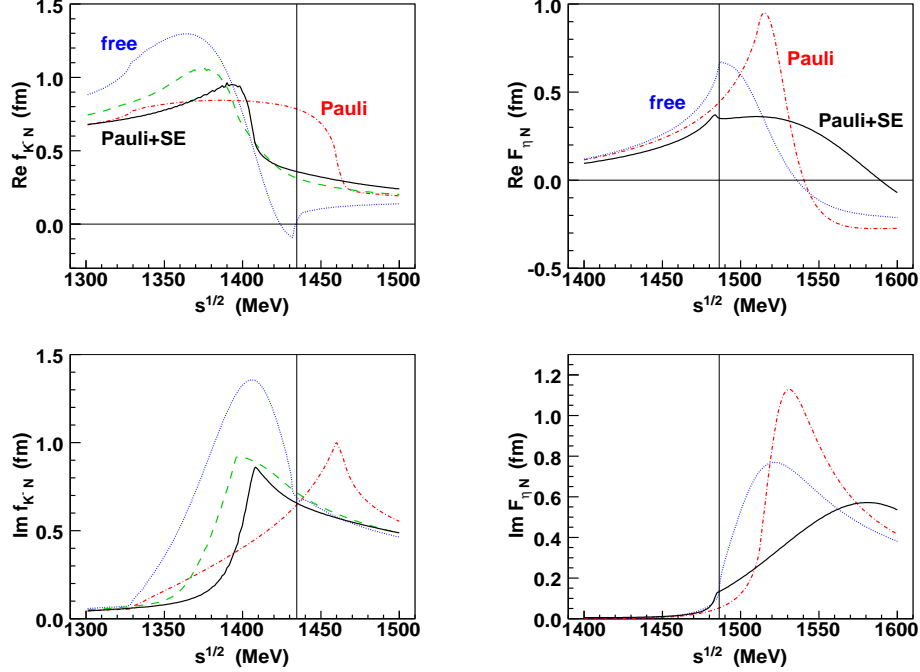


Fig. 3. Left: near-threshold energy dependence of K^-N cm reduced scattering amplitudes in model NLO30 of Ref. [19] for free-space (dotted) and Pauli-blocked amplitudes at $\rho = \rho_0$ with (solid) and without (dot-dashed) meson and baryon self-energies (SE). The dashed curves show Pauli-blocked amplitudes with SE at $\rho = 0.5\rho_0$. Right: energy dependence of ηN free-space and in-medium (at ρ_0) cm scattering amplitudes across threshold and beyond the $N^*(1535)$ resonance in model NLO30 $_\eta$ of Ref. [15]. The K^-N and ηN thresholds are marked by thin vertical lines.

where $\xi_{N(h)} \equiv m_{N(h)}/(m_N + m_h)$. Using the Fermi Gas model for nucleons and the local density approximation, one gets

$$\delta\sqrt{s} \approx -B_N \frac{\rho}{\bar{\rho}} - \xi_N B_h \frac{\rho}{\rho_0} - \xi_N T_N \left(\frac{\rho}{\rho_0}\right)^{2/3} - \xi_h \frac{\sqrt{s}}{\omega_h E_N} 2\pi \text{Re } F_{hN}(\sqrt{s}, \rho) \rho, \quad (7)$$

where $T_N = 23.0$ MeV at nuclear-matter density ρ_0 , $B_N \approx 8.5$ MeV is an average nucleon binding energy and $\bar{\rho}$ is the average nuclear density. For the charged K^- meson, a Coulomb term proportional to $V_C \times (\rho/\rho_0)^{1/3}$ was added [9]. Expression (7) respects the low-density limit, $\delta\sqrt{s} \rightarrow 0$ upon $\rho \rightarrow 0$. For attractive scattering amplitudes, all four terms in Eq. (7) are negative definite, the last one providing substantial downward energy shift overlooked by many previous calculations that assumed $\vec{p}_h = 0$ which

is inappropriate for *finite* nuclei. Since \sqrt{s} depends through Eq. (7) on $\text{Re } F_{hN}(\sqrt{s}, \rho)$ which by itself depends on \sqrt{s} , it is clear that for a given value of B_h , $F_{hN}(\sqrt{s}, \rho)$ has to be determined *self-consistently* by iterating Eq. (7). This is done at each radial point where ρ is given, and for each B_h value during the calculation of bound states. The emerging correlation between the downward energy shift $\delta\sqrt{s}$ and the density ρ renders $F_{hN}(\sqrt{s}, \rho)$ into a state-dependent function of the density ρ alone, denoted for brevity by $F_{hN}(\rho)$. This correlation is shown on the left panel of Fig. 4 for kaonic atoms, where $B_{K^-} \approx 0$, and on the right panel for the $1s_\eta$ nuclear bound state in Ca. The figure demonstrates appreciable energy shifts below threshold in both kaonic atoms and η -nuclear bound states, amounting to 40 MeV at $0.5\rho_0$.

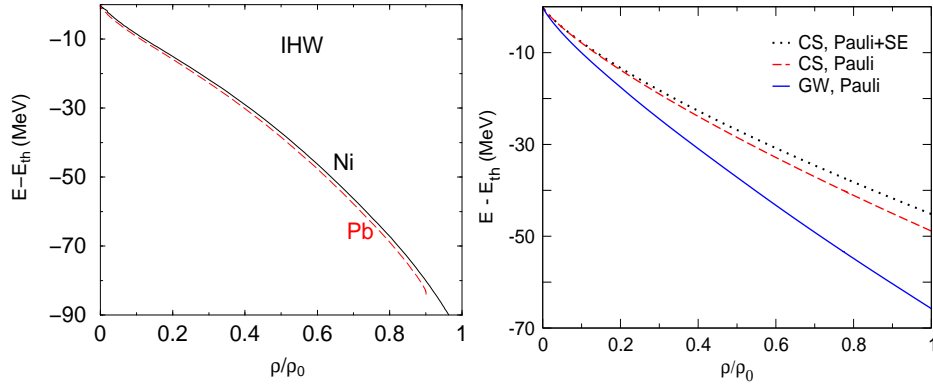


Fig. 4. Subthreshold energies probed in kaonic atoms of Ni and Pb (left panel) and for a $1s_\eta$ bound state in Ca (right panel) as a function of nuclear density, calculated self-consistently within the IHW-based global fit to kaonic atoms [9] and for in-medium ηN scattering amplitudes constructed from the meson-baryon models GW and CS in Ref. [11].

3. K^- interactions in kaonic atoms

The most recent kaonic-atom calculations are due to Friedman and Gal in Ref. [7], using in-medium K^-N scattering amplitudes generated in model NLO30 of Cieplý and Smejkal [19] as described in the previous section, and in Ref. [9] using Pauli blocked K^-N scattering amplitudes generated from the free-space NLO scattering amplitude of Ikeda, Hyodo and Weise [18]. The CS [19] and IHW [18] free-space amplitudes $F_{K^-N}(\sqrt{s})$ agree semi-quantitatively with each other. The kaonic-atom fit in Ref. [9] considers in addition to the input in-medium IHW-based one-nucleon (1N)

amplitude $F_{K-N}(\sqrt{s}, \rho)$ also many-nucleon absorptive and dispersive contributions, represented by energy-independent phenomenological amplitude $F_{K-N}^{\text{many}}(\rho)$ with prescribed density dependence form that includes several fit parameters. The assumption of energy independence is motivated by observing that K^- absorption on two nucleons, which is expected to dominate F_{K-N}^{many} , releases energy $\sim m_{K^-}$ considerably larger than the subthreshold energies of less than 100 MeV encountered in kaonic-atom calculations. The self-energy input Π_{K^-} to the KG equation (5) is now constructed from an *effective* K^-N scattering amplitude $F_{K-N}^{\text{eff}} = F_{K-N}^{\text{one}} + F_{K-N}^{\text{many}}$ which is iterated through the self-consistency expression (7). This introduces coupling between the many-nucleon fitted amplitude F_{K-N}^{many} and the converged one-nucleon amplitude F_{K-N}^{one} that evolves from the 1N input amplitude $F_{K-N}(\rho)$: $F_{K-N}^{\text{one}}(\rho) \rightarrow F_{K-N}^{\text{one}}(\rho)$ upon $F_{K-N}^{\text{many}} \rightarrow 0$.

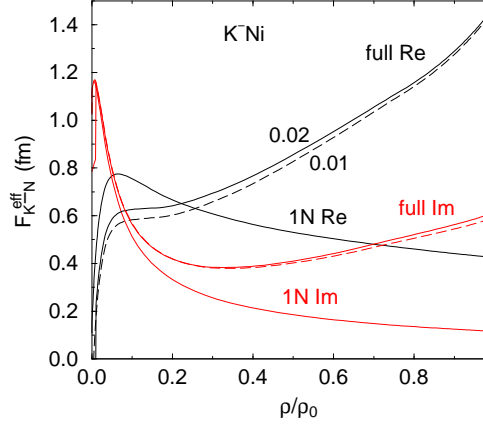


Fig. 5. Kaonic-atom globally fitted amplitude $F_{K-N}^{\text{eff}}(\rho)$, marked “full”, and the in-medium IHW-based amplitude $F_{K-N}(\rho)$ in the absence of many-nucleon contributions, marked “1N”, as a function of nuclear density in Ni. Solid (dashed) curves are for matching to free-space amplitudes at 0.02(0.01) ρ_0 .

The full effective amplitude $F_{K-N}^{\text{eff}}(\rho)$ resulting from the global kaonic-atom fit in [9] is shown in Fig. 5 marked “full”, along with the in-medium IHW-based amplitude $F_{K-N}(\rho)$ marked “1N”. The figure makes it clear that for densities exceeding $\sim 0.5\rho_0$ the full effective amplitude departs appreciably from the in-medium IHW-based amplitude, which in the case of the imaginary part amounts to doubling the 1N absorptivity of in-medium K^- mesons. For a more details we refer the reader to Ref. [9].

The K^- nuclear attraction and absorptivity deduced from global kaonic-atom fits are sizable at central nuclear densities. This is demonstrated

by the real and imaginary parts of the potential V_{K^-} plotted for Ni in Fig. 6. Although the potential depths might reflect a smooth extrapolation provided by the input components of the K^-N amplitudes, the potential at $0.5\rho_0$ and perhaps up to $0.9\rho_0$ is reliably determined in kaonic-atom fits [20]. It is reassuring that both IHW-based and NLO30-based fits agree with each other semi-quantitatively as shown on the left panel.

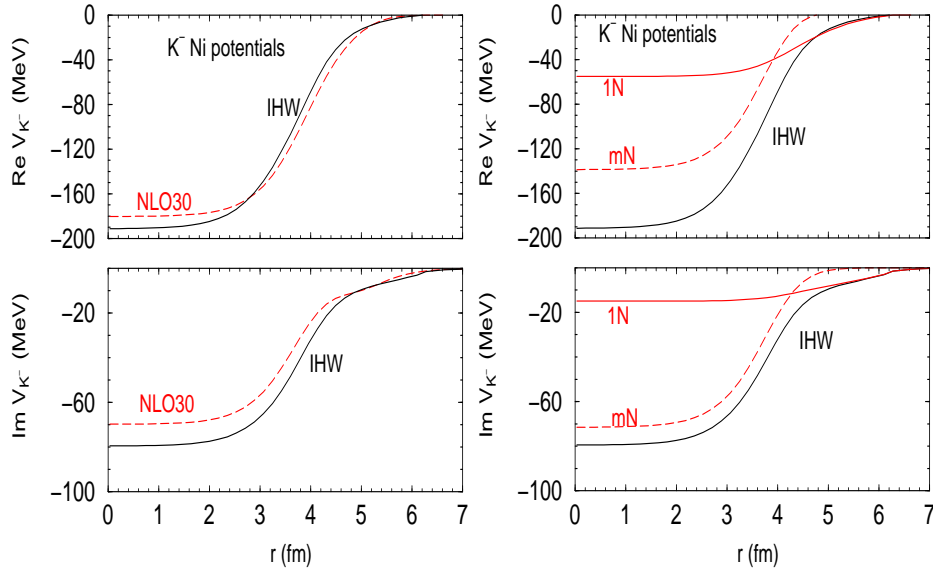


Fig. 6. Left: K^- nuclear potentials for K^- atoms of Ni derived from global fits based on in-medium IHW amplitudes [9], with the corresponding 1N and many-nucleon (mN) components on the right panel. The dashed curves in the left panel are derived from in-medium NLO30 amplitudes [7]. The rms radius of the input Ni density is 3.72 fm.

The right panel of Fig. 6 shows a non-additive splitting of the fitted K^- -nuclear potential into a 1N in-medium component, obtained on the assumption that there is no many-nucleon (mN) component present, and a fitted mN component. The breakdown of the imaginary part of the potential is of particular interest, indicating that the mN component which is sizable in the nuclear interior becomes negligible about half a fermi outside of the half-density radius. This has implications for choosing optimally kaonic-atom candidates where widths of two atomic levels can be measured so as to substantiate the 1N vs mN pattern observed in global fits [21].

4. Few-body kaonic quasibound states

For K^- -nuclear three- and four-body calculations, a variant of the downward energy shift Eq. (7) derived for many-body calculations was formulated by Barnea, Gal and Liverts [6]:

$$\delta\sqrt{s} = -\frac{B}{A} - \frac{A-1}{A}B_K - \xi_N \frac{A-1}{A} \langle T_{N:N} \rangle - \xi_K \left(\frac{A-1}{A} \right)^2 \langle T_K \rangle, \quad (8)$$

with A the baryonic number, B the total binding energy of the system, $B_K = -E_K$, T_K the kaon kinetic energy operator in the total cm frame and $T_{N:N}$ the pairwise NN kinetic energy operator in the NN pair cm system. Note that $\delta\sqrt{s}$ is negative-definite by expression (8) which provides a self-consistency cycle upon requiring that \sqrt{s} derived through Eq. (8) from the solution of the Schroedinger equation agrees with the value of \sqrt{s} used for the input $V_{\bar{K}N}(\sqrt{s})$. Total binding energies calculated variationally in the hyperspherical basis are shown in Fig. 7 for three- and four-body kaonic bound states. Details of the input chirally-based energy-dependent $\bar{K}N$ interactions and the actual calculations of these few-body kaonic clusters are given in Ref. [6].

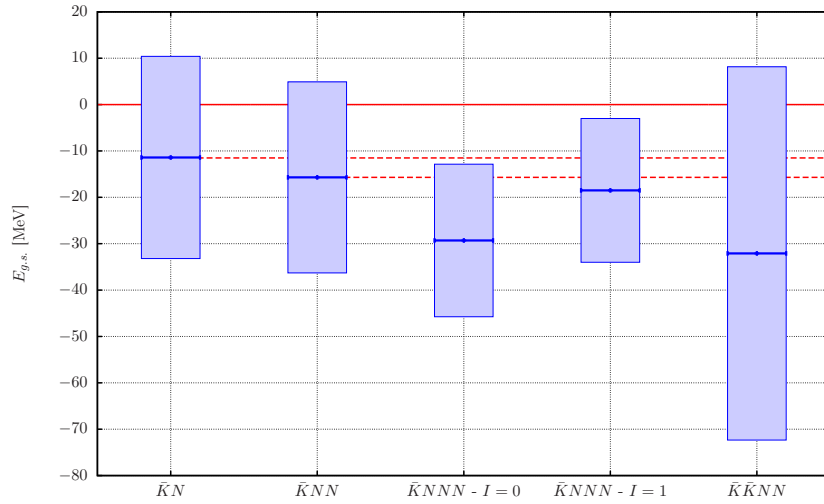


Fig. 7. Calculated binding energies and $\bar{K}N \rightarrow \pi Y$ widths of \bar{K} and $\bar{K}\bar{K}$ few-body quasibound states [6] in MeV. Horizontal lines denote particle-stability thresholds. Widths are represented by vertical bars.

Shown also as vertical bars in Fig. 7 are $\bar{K}N \rightarrow \pi Y$ width estimates using the approximation

$$\frac{\Gamma}{2} \approx \langle \Psi_{\text{g.s.}} | -\text{Im } \mathcal{V}_{\bar{K}N} | \Psi_{\text{g.s.}} \rangle, \quad (9)$$

where $\mathcal{V}_{\bar{K}N}$ consists of all pairwise $\bar{K}N$ interactions. Expression (9) provides a good approximation owing to $|\text{Im } \mathcal{V}_{\bar{K}N}| \ll |\text{Re } \mathcal{V}_{\bar{K}N}|$ [22]. Expressions similar to (8) and (9) were used in $\bar{K}\bar{K}NN$ calculations. With $\bar{K}N$ input interactions that become weaker upon going subthreshold [22], and owing to the self-consistency requirement, the calculated binding energies (widths) come out typically 10 (10–40) MeV lower than for threshold input interactions $V_{\bar{K}N}(\sqrt{s_{\text{th}}})$. In particular, the $I = 1/2$ $\bar{K}NN$ g.s., known as ‘ K^-pp ’, lies only 4.3 MeV below the 11.4 MeV centroid of the $I = 0$ $\bar{K}N$ quasibound state, the latter value differing substantially from the 27 MeV binding energy assigned traditionally to the $\Lambda(1405)$ resonance (and used in non-chiral calculations). The widths exhibited in the figure, of order 40 MeV for single- \bar{K} clusters and twice that for double- \bar{K} clusters, are due to $\bar{K}N \rightarrow \pi Y$. Additional $\bar{K}NN \rightarrow YN$ contributions of up to ~ 10 MeV in K^-pp [23] and ~ 20 MeV in the four-body systems [6] are foreseen.

5. Many-body kaonic quasibound states

In-medium $\bar{K}N$ scattering amplitudes derived from the chirally motivated NLO30 model by CS [19] were used by Gazda and Mareš [8] to evaluate K^- quasibound states across the periodic table, with binding energies and widths shown in Fig. 8. The phenomenological mN amplitudes derived from fitting kaonic-atom data, as described in Sect. 3, are not included in these calculations. The left panel demonstrates a robust pattern of K^- -nuclear binding owing to the strongly attractive in-medium K^-N scattering amplitude shown in Fig. 3, in agreement with previous calculations by Weise and collaborators who used a less advanced form of the $\delta\sqrt{s}$ self-consistency requirement [24]. Several K^- quasibound states are predicted to exist in a given nucleus, except for the very light nuclei, but as suggested by the corresponding widths shown on the right panel these states are likely to be too broad to be uniquely resolved.

The hierarchy of widths shown for a given nucleus in Fig. 8 is also worth noting. For energy independent potentials one expects maximal widths in the lowest, most localized $1s_K$ states, and gradually decreased widths in excited states which are less localized within the nucleus. The reverse is observed on the right panel of the figure. This is a corollary of requiring self consistency: the more excited a K^- quasibound state is, the lower nuclear density it feels, and a smaller downward shift into subthreshold

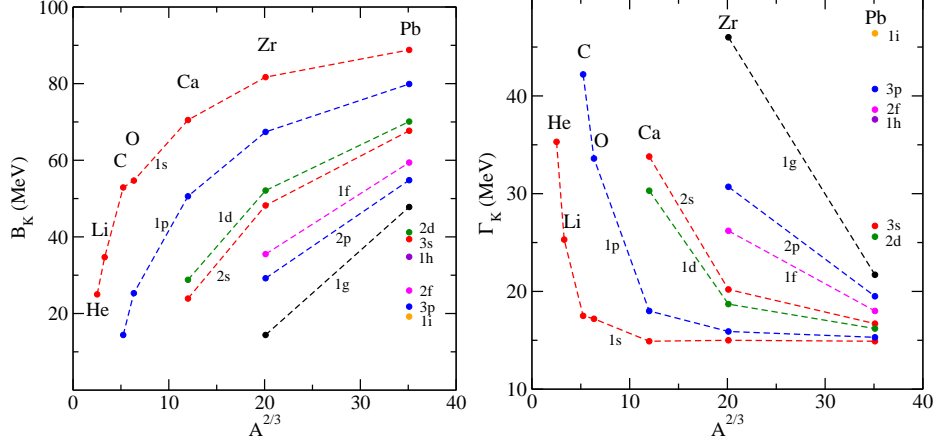


Fig. 8. K^- Binding energies B_K (left) and widths Γ_K (right) calculated self-consistently using NLO30-based in-medium K^-N subthreshold amplitudes and static RMF densities [8].

energies it probes via the $s(\rho)$ dependence. Since by Fig. 3 $\text{Im } f_{K-N}(\rho)$ decreases strongly upon going below threshold, its contribution to the calculated width gets larger, the higher the excited quasibound-state energy is. Additional width contributions from mN processes are found to increase appreciably the calculated widths, with estimates made in Ref. [8] for the overall width of K^- quasibound states in Ca, for example, in the range of values $\Gamma_K \sim (50 - 70)$ MeV.

6. η -nuclear quasibound states

It was noted in Sect. 1 that free-space near-threshold ηN scattering amplitudes $F_{\eta N}(\sqrt{s})$ are highly model dependent, as demonstrated in Fig. 2 for four of the many amplitudes available in the literature. Since the amplitudes denoted there GW [14] and M2 (also M1) [16] are available only in free-space versions, appropriate in-medium versions have been produced in Ref. [10] by applying the Ericson-Ericson multiple-scattering renormalization [25]:

$$F_{\eta N}(\sqrt{s}, \rho) = \frac{F_{\eta N}(\sqrt{s})}{1 + \xi(\rho)(\sqrt{s}/m_N)F_{\eta N}(\sqrt{s})\rho}, \quad (10)$$

where $p_F = (3\pi^2\rho/2)^{1/3}$ is the local Fermi momentum corresponding to density ρ and $\xi(\rho) = 9\pi/4p_F^2$ accounts for Pauli blocking at threshold. These in-medium amplitudes were then used as input within self-consistent

calculations, as described in Sect. 2. In the left panel of Fig. 9 we show $1s_\eta$ -nuclear widths calculated in these models. Whereas model GW generates widths smaller than 5 MeV, the widths in models M are twice (M2) and five times (M1) as large. This demonstrates clearly that the calculated η -nuclear widths are not related directly to $\text{Im } a_{\eta N}$, the imaginary part of the scattering length which is approximately the same in all these models. The difference between the calculated sequences of widths is in fact due to the difference between the subthreshold free-space imaginary parts of the amplitudes shown in the right panel of Fig. 2, in spite of their near equality at threshold.

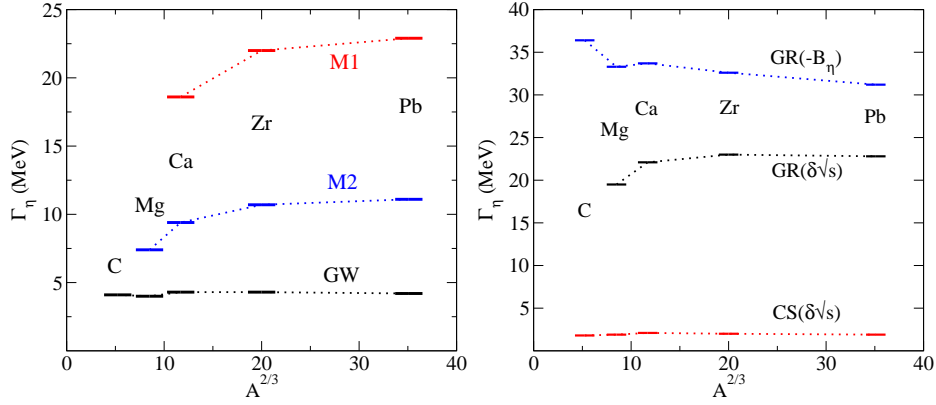


Fig. 9. Calculated widths of $1s_\eta$ nuclear bound states are shown on the left panel for in-medium GW [14] and M [16] versions of ηN scattering amplitudes, and on the right panel for the in-medium versions CS [11] and GR [26], the latter is based on the free-space model IOV [17] and its in-medium extension [27].

In-medium versions that account for Pauli blocking and self-energies are available for the other two model amplitudes CS [15] and IOV [17] shown in Fig. 2. These in-medium versions, marked CS and GR [26] respectively in Fig. 9, have been discussed extensively in Ref. [11] with calculated $1s_\eta$ -nuclear widths shown on the right panel of the figure. In this plot, calculations using the self-consistency requirement (7) are denoted $\delta\sqrt{s}$ and the GR calculations that used a density-independent $\delta\sqrt{s} = -B_\eta$ self-consistency requirement are denoted $-B_\eta$. The calculated GR widths are considerably larger than those due to CS, which again results from the difference between the subthreshold free-space imaginary parts of the amplitudes shown on the right panel of Fig. 2, in spite of their near equality at threshold. It is also seen that applying the $\delta\sqrt{s}$ procedure instead of their original $-B_\eta$ procedure leads to appreciable reduction of the calculated GR widths. The main

conclusion drawn from Fig. 9 is that, while models GW and CS produce sufficiently small η -nuclear widths, it will be prohibitively difficult to resolve η -nuclear states if the correct underlying ηN amplitudes are due to models M1, M2 or GR. The widths presented in Fig. 9 do not include contributions from two-nucleon processes which are estimated to add a few MeV [28].

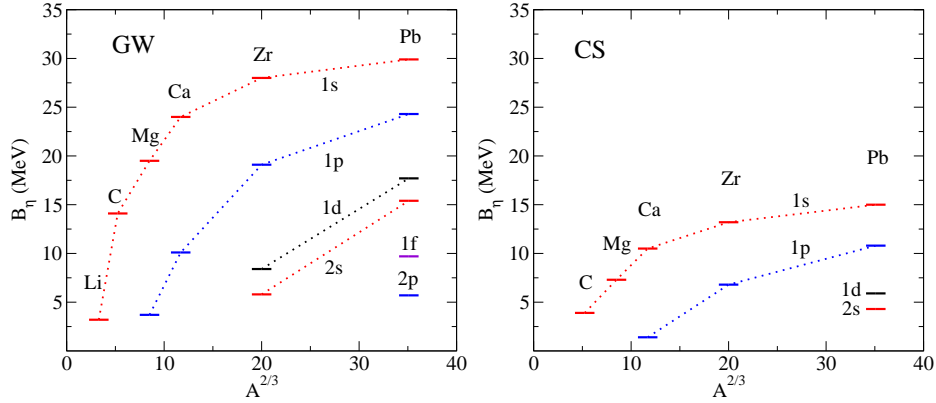


Fig. 10. Spectra of η -nuclear single-particle bound states across the periodic table, calculated self-consistently using in-medium models of the ηN subthreshold scattering amplitude, are shown in the left panel for the GW model [14] and in the right panel for the NLO30 $_{\eta}$ model of CS [15]. Pauli blocking is included for both in-medium models, whereas hadron self-energies are accounted for only in the CS-based calculations.

Finally, in Fig. 10 we show η -nuclear single-particle spectra across the periodic table, evaluated for models GW and CS in which the calculated widths turned out to be sufficiently small to resolve individual bound states. Both in-medium versions of these models account for Pauli blocking, whereas CS also accounts for hadron self-energies, resulting in 2–3 MeV lower binding energies relative to those calculated with only Pauli blocking.

7. Summary and outlook

In this overview of \bar{K}^- - and η -nuclear bound-state calculations we have focused on the role played by the underlying meson-baryon subthreshold dynamics. It was shown how the energy dependence of the meson-baryon in-medium scattering amplitudes is converted into density dependence of the meson self-energies, or equivalently of meson-nucleus optical potentials. Based on global fits of K^- -atom data we argued that in-medium chiral model input has to be supplemented by appreciable many-nucleon dispersive and absorptive potential contributions which imply uniformly large widths

of order 50 MeV and more for \bar{K} -nuclear bound states, except perhaps for the very light few-body systems. Smaller widths, of order 20 MeV or less, were calculated for η -nuclear bound states. This will make it difficult to identify uniquely such states in forthcoming experiments, unless the underlying ηN physics corresponds to models such as GW or CS. Furthermore, the in-medium subthreshold amplitudes encountered in η -nuclear bound-state calculations are substantially weaker both in their real part as well as in their imaginary part than the ηN scattering length. This weakening of the real part makes the binding of η in very light nuclei such as ^3He and ^4He improbable, except perhaps in model GW. However, the methodology of constructing and using η -nuclear potentials does not fit into realistic few-body calculations which require separate treatment. To date, in spite of several experimental searches for η -nuclear bound states, particularly in the He isotopes (for the most recent report see Ref. [29]), the only claim of observing such a bound state is in the reaction $p + ^{27}\text{Al} \rightarrow ^3\text{He} + ^{25}_{\eta}\text{Mg} \rightarrow ^3\text{He} + p + \pi^- + X$, reported by the COSY-GEM collaboration [30].

Acknowledgements

A.G. would like to thank Pawel Moskal for the invitation to participate in the Mesic Nuclei symposium and for his kind hospitality. This work was supported by the GACR Grant No. 203/12/2126, as well as by the EU initiative FP7, HadronPhysics3, under the SPHERE and LEANNIS cooperation programs.

REFERENCES

- [1] S. Wycech, Nucl. Phys. B 28 (1971) 541.
- [2] W.A. Bardeen, E.W. Torigoe, Phys. Lett. B 38 (1972) 135.
- [3] J.R. Rook, Nucl. Phys. A 249 (1975) 466.
- [4] A. Cieplý, E. Friedman, A. Gal, D. Gazda, J. Mareš, Phys. Lett. B 702 (2011) 402, Phys. Rev. C 84 (2011) 045206.
- [5] A. Cieplý, E. Friedman, A. Gal, V. Krejčířík, Phys. Lett. B 698 (2011) 226.
- [6] N. Barnea, A. Gal, E.Z. Liverts, Phys. Lett. B 712 (2012) 132.
- [7] E. Friedman, A. Gal, Nucl. Phys. A 881 (2012) 150.
- [8] D. Gazda, J. Mareš, Nucl. Phys. A 881 (2012) 159.
- [9] E. Friedman, A. Gal, Nucl. Phys. A 899 (2013) 60.
- [10] E. Friedman, A. Gal, J. Mareš, Phys. Lett. B 725 (2013) 334.
- [11] A. Cieplý, E. Friedman, A. Gal, J. Mareš, Nucl. Phys. A 925 (2014) 126.
- [12] Z.-H. Guo, J.A. Oller, Phys. Rev. C 87 (2013) 035202.

- [13] M. Bazzi, et al., SIDDHARTA Collaboration, Phys. Lett. B 704 (2011) 113, Nucl. Phys. A 881 (2012) 88.
- [14] A.M. Green, S. Wycech, Phys. Rev. C 71 (2005) 014001.
- [15] A. Cieplý, J. Smejkal, Nucl. Phys. A 919 (2013) 46.
- [16] M. Mai, P.C. Bruns, U.-G. Meißner, Phys. Rev. D 86 (2013) 094033.
- [17] T. Inoue, E. Oset, M.J. Vicente Vacas, Phys. Rev. C 65 (2002) 035204.
- [18] Y. Ikeda, T. Hyodo, W. Weise, Phys. Lett. B 706 (2011) 63, Nucl. Phys. A 881 (2012) 98.
- [19] A. Cieplý, J. Smejkal, Nucl. Phys. A 881 (2012) 115.
- [20] N. Barnea, E. Friedman, Phys. Rev. C 75 (2007) 022202(R).
- [21] E. Friedman, S. Okada, Nucl. Phys. A 915 (2013) 170.
- [22] T. Hyodo, W. Weise, Phys. Rev. C 77 (2008) 035204.
- [23] A. Doté, T. Hyodo, W. Weise, Nucl. Phys. A 804 (2008) 197, Phys. Rev. C 79 (2009) 014003.
- [24] W. Weise, R. Härtle, Nucl. Phys. A 804 (2008) 173.
- [25] T. Waas, M. Rho, W. Weise, Nucl. Phys. A 617 (1997) 449.
- [26] C. García-Recio, T. Inoue, J. Nieves, E. Oset, Phys. Lett. B 550 (2002) 47.
- [27] T. Inoue, E. Oset, Nucl. Phys. A 710 (2002) 354.
- [28] S. Wycech, Acta Phys. Polon. B 41 (2010) 2201.
- [29] P. Adlarson, et al. (WASA-at-COSY Collaboration), Phys. Rev. C 87 (2013) 035204.
- [30] A. Budzanowski, et al. (COSY-GEM Collaboration), Phys. Rev. C 79 (2009) 012201(R).